Int. J. Electrochem. Sci., 15 **(2020)** 6464 – 6477, doi: 10.20964/2020.07.48

International Journal of
ELECTROCHEMICAL
SCIENCE
www.electrochemsci.org

Corrosion Behavior of Low-Carbon Steel and Weathering Steel in a Coastal Zone of the Spratly Islands: A Tropical Marine Atmosphere

Yuwei Liu[1,2], *Hongtao Zhao*[1], *Zhenyao Wang*[1,*], *Yinghua Wei*[1], *Chen Pan*[1], *Chenxi Lv*[1]

[1] Institute of Metal Research, Chinese Academy of Sciences, Wencui Rd 62, Shenyang, 110016, China
[2] School of Materials Science and Engineering, University of Science and Technology of China, Wencui Rd 62, Shenyang, 110016, China
[*]E-mail: zhywang@imr.ac.cn

Received: 7 March 2020 / *Accepted:* 11 April 2020 / *Published:* 10 June 2020

For the first time, the initial atmospheric corrosion behavior of low-carbon steel and weathering steel, exposed in a tropical marine zone of the Spratly Islands, has been examined over one year. The results indicated that the corrosion products were mainly composed of β–FeOOH, α–FeOOH, γ–FeOOH, and Fe_3O_4. The transformation between each phase and the cracking, linearly arrayed voids distributed in the rust layer together promoted the corrosion process. The kinetics of both steels exhibited an accelerating process following the exponential function $D = At^n$. In terms of the corrosion rate, r_{corr}, for the first year of exposure to different corrosivity categories defined in ISO 9223, that of the low-carbon steel Q235 exposed in the Spratly Islands was 237.5 μm/a; therefore, the corrosivity category of this marine atmosphere was CX.

Keywords: Low-carbon steel Q235; Weathering steel Q450NQR1; Corrosion depth; Spratly Islands; Atmospheric corrosion

1. INTRODUCTION

The atmospheric corrosion of carbon steel is a noteworthy problem throughout the world, particularly in coastal areas. Carbon steel has become widely used in construction, transportation, and also as reinforcement steel in reinforced concrete structures. Nowadays, the loss of metals due to atmospheric corrosion accounts for more than half of the total corrosion of the materials. Therefore, many studies have been conducted on the atmospheric corrosion behavior of carbon steel over many years [1-9]. These studies have mainly focused on rural, industry, and marine atmospheres, for which pollutants have been shown to have a significant impact on the corrosion process. In rural atmospheres, the corrosion rate is the lowest owing to low atmospheric pollution, whereas in urban or industrial

atmospheres, the corrosion process is influenced by the SO_2 concentration [10, 11]. The existence of SO_2 can cause the surface morphology of corrosion products to form a nest structure, in which the ratio of α/γ changes with SO_2 pollution content [12]. When the air contains both Cl^- and SO_2, the corrosion process is quite different owing to the synergic effect of the combined influence of SO_2 and chlorides or the competitive absorption of SO_2 and chlorides [13, 14]. In a marine atmosphere, Cl^- deposition is the main factor affecting the corrosion process, as the concentration of Cl^- determines the structure of the rust layer formed on carbon steel and the composition of corrosion products [8, 15, 16].

In addition to pollutants, temperature, humidity, solar radiation, and wind speed all have certain influences on the corrosion process. Each typical atmospheric environment has its own peculiarities. Owing to its location near the equator and the direct impact of solar radiation, the tropical marine atmosphere is a typical climate with high temperature, high humidity, high salinity, and high radiation. However, little research has been carried out in this climate so far. In the last few years, some studies [8, 17, 18] have been conducted in South America, such as Valparaiso Bay, Chile, Havana, Cuba, and Medellin, Colombia. However, in middle-south Asia, there has been very little corrosion data. Spratly Islands, located in the southernmost part of China, is a zone of high construction potential and tourist development. Many steel components, including those used as rebar and bridge steel, are significantly influenced by atmospheric corrosion. The service life of a material is usually closely related to the corrosivity category of its environment. However, the corrosivity category of this region has not been reported so far. A method for predicting the corrosion classification of the atmospheric environment is provided in ISO 9223—one method is based on the corrosion rate of metal standard specimens exposed in a natural environment after one year, whereas the other method is based on the concentration of SO_2 in an atmospheric environment, amount of Cl^- deposition, and wetting time to form a speculative corrosion classification.

Estimating atmospheric corrosion solely from environmental databases without natural corrosion tests in an actual atmospheric environment involves long waiting times, considerable expense, and an acceptance that errors will occur at times. Because of low price, carbon steel is often used as a ferrous metal to evaluate the corrosivity of the atmospheric environment. Therefore, it is important to characterize the atmospheric corrosion behavior of carbon steel in the coastal tropical zone of the Spratly Islands over a short time.

2. MATERIAL AND METHODS

2.1 Materials preparation

Low-carbon steel Q235 and weathering steel Q450NQR1 were chosen as the testing materials, with the chemical compositions given in Table 1. The coupons of both carbon steels were cut into 100 mm × 200 mm × 5.5 mm samples, and the six faces were mechanically polished to 0.8 Ra. Four parallel samples were used for the same exposure time, three were used for weight-loss analysis, and one for rust-layer analysis. Before outdoor exposure, the carbon steel plates were numbered, ultrasonically cleaned with acetone, dried, stored for 24 h, and then weighed (original weight).

Table 1. Chemical composition of carbon steel (wt. %)

	C	Si	Mn	P	S	Cr	Ni	Cu
Q235	0.22	0.08	0.10	0.015	0.003	-	-	-
Q450NQR1	0.08	0.31	0.41	0.073	0.006	0.47	0.15	0.29

2.2 Field exposure test

The exposure site is located in the Spratly Islands about 150 m far away from the coastline, 9°54′ northern latitude and 115°32′ eastern longitude, a tropical marine climate. The climatic characterization and the main environmental parameters are listed in Table 2. The average atmospheric temperature in Spratly Islands was 28.1 ℃ with a maximum temperature of 34.7 ℃, and the temperature difference during the day was 2.3 ℃, a relatively high temperature. The extreme relative humidity values ranged between 77% and 88% with a mean value of 81.6%, a relatively high humidity. The carbon plates were exposed to the south with an angle of 45° to the horizontal of the sky. All the coupons were prepared uniformly and exposed on September 1, 2017. Four replicate metal samples were retrieved from the island for analyses after 0.5, 1, 2, 5, and 12 months of exposure. For gravimetric experiments, the corrosion products formed on retrieved samples were first scraped by a razor blade and then immersed in a solution of 500-mL HCl, 500-mL distilled water and 3-g hexamethylenetetramine at 20 ℃ until the products were totally removed. After corrosion products were removed, the samples were rinsed with distilled water and alcohol, then dried and weighted.

Table 2. Experimental conditions of exposure location

Average temperature (℃/year)	Average relative humidity (%)	Average rainfall (mm/year)	Rain days (days/year)	Average total solar radiation (W/m^2)
28.1	81.6	2000	210	10

2.3 Analysis of corrosion products

The macro-morphology of the rusted samples was observed by digital camera and the micro-morphology of the cross section was revealed by scanning electron microscopy (SEM, FEI QUANTA 450). The composition of the rust layer was analyzed using qualitative and quantitative XRD. Two tests were both obtained using Rigaku-D/max 2000PC with a Cu-Kα target at 50 kV and 300 mA ranging from 10° to 70°. For qualitative analysis, the scanning speed was 10 $deg \cdot min^{-1}$. For quantitative analysis, the scanning speed was 1 $deg \cdot min^{-1}$, and the data were analyzed using Maud software to determine the relative content of each corrosion product.

2.4 Electrochemical measurements

The tested samples were manually cut from the entire rusted coupons, connected with a copper conductor, and mounted in rosin paraffin with an exposure area of 1 cm^2. Potentiodynamic polarization measurements were performed with a PARSTAT 2273 potentiostat/galvanostat and traditional three-electrode cell at room temperature. The rusted samples served as a working electrode, a large platinum plate served as the counter electrode, and a saturated calomel electrode (SCE) served as the reference electrode. Because of its stability and its minimal effect on the original properties of the rust layer, 0.1-mol/L Na_2SO_4 was chosen as the electrolyte. The rusted samples were immersed in the electrolyte until a stable corrosion potential was obtained; then, potentiodynamic polarization measurements were carried out at a scanning rate of 0.33 mV/s and a scan range of −0.25 V (vs.OCP) to 0 V. All potential values mentioned in this paper are with reference to SCE in saturated KCl solution.

3. RESULTS AND DISCUSSION

3.1 Corrosion kinetics of low-carbon steel Q235 and weathering steel Q450NQR1

The corrosion depth is usually used to evaluate the corrosion kinetics of carbon steel due to uniform corrosion behavior. It can be calculated as

$$D=\frac{10000(w_0-w_1)}{\rho S}\ , \qquad (1)$$

where D is the corrosion depth (μm), w_0 is the original weight (g), w_1 is the final weight (g), ρ is the density of the carbon steel (7.86 g/cm^3), and S is the total area of the six surfaces (433 cm^2). **Figure 1**(a) shows the corrosion depth of Q235 and Q450NQR1 during 12-month exposure in Spratly Islands marine atmosphere. It can be seen apparently that the corrosion depth of both Q235 and Q450NQR1 increased at different degrees with exposure time, and the corrosion depth of Q235 was much greater than that of Q450NQR1 after 5-month exposure.

In general, the corrosion depth of metals exposed to the open air also follows the well-known exponential function, to which all data were regressed using Equation (2).

$$D=At^n\ , \qquad (2)$$

where D is the corrosion depth (μm), t is the exposure time (month), and A and n are constants. Figure 1(a) shows both the regression curves and the actual data. The value of A was almost the same for both steels, indicating the same vulnerability to rusting at the beginning of the exposure and also verifying that the value of A fluctuated a little with change in the composition of alloying elements [19]. The value of n directly reflects the protection of the rust layer. As reported in previous studies, the value of n was mostly in the range from 0.3 to 0.6, most of the highest value of n ever reported was 1.0 by Shastry et al. [3], only a few areas had values of $n > 1$[1]. In this study, the n values of Q235 and Q450NQR1 were 1.41 and 1.08, respectively, with both corrosion processes exhibiting accelerated trends owing to $n > 1$. As known, the larger the n value is, the poorer the protectiveness is; that is to say, the accelerated rate of Q235 was much higher than that of Q450NQR1. Compared with other marine atmospheric environments [1, 20, 21], the corrosion depths after 1-year exposure at this site were greater

than those at most areas, such as Wanning, Qingdao, China, and Bohus Malmon Kvarnvik, Sweden. The high value of *n* depends on the high temperature (annual average temperature of 28.1 °C) and high humidity (ranging from 77% to 88%), and is also affected by marine pollution.

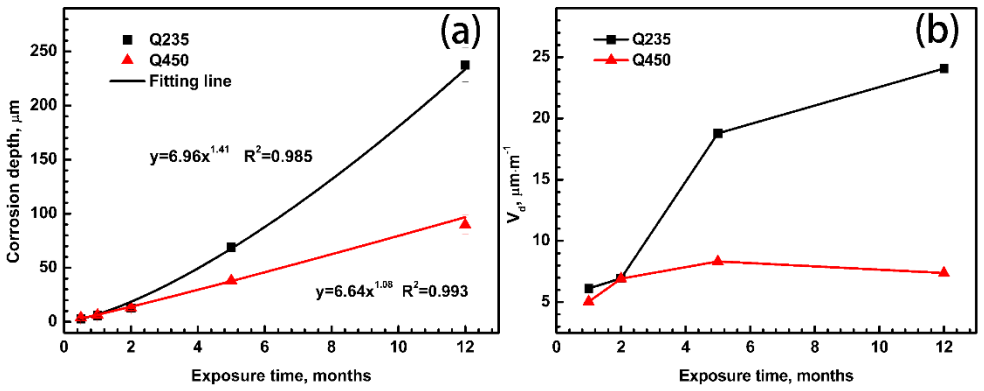

Figure 1. Variation of the corrosion depth and the corrosion rate of Q235 and Q450NQR1 as function of exposure time.

According to corrosion rate, r_{corr}, for the first year of exposure for different corrosivity categories defined in ISO 9223, r_{corr} of low-carbon steel Q235 exposed in the Spratly Islands was 237.5 μm/a; therefore, the corrosivity category of this marine atmosphere is CX, belonging to an extreme environment. Paracel Islands and the Spratly Islands are both atmospheric environments of the South China Sea; however, the corrosion rate of low-carbon steel Q235 exposed to Paracel Islands was 126.45 μm/a, which was half the corrosion rate in our study (237.5 μm/a); thus, the corrosion process of low-carbon steel Q235 exposed in the Spratly Islands cannot be extrapolated from the existing data. To get further information about the corrosion process, the average corrosion rate (V_d) after exposure for different periods was calculated by using the following equation,

$$V_d = \frac{D_n - D_{n-1}}{t_n - t_{n-1}}, \qquad \text{(Eq. 3)}$$

where V_d is the corrosion rate (μm/month), D_n and t are the corrosion depth (μm) and exposure time (month), and n is the period (n = 1, 2, 3, 4, 5 refer to samples exposed for 0.5, 1, 2, 5, and 12 months, respectively). Figure 1(b) shows the corrosion rates of Q235 and Q450NQR1 as function of exposure time. It can be seen that the variation trends of the corrosion rate of the two materials were similar but different. The corrosion rate of Q235 increased continuously during the 12-month exposure, whereas the corrosion rate of Q450NQR1 first increased and then decreased slightly after 12-month exposure. Many studies [2, 22] have indicated that it usually takes more than 3 years to form a protective rust layer on the surface of weathering steel. However, in this tropical marine atmosphere, the corrosion rate of weathering steel (89.75μm/a) was much smaller than that of low-carbon steel Q235 (237.5 μm/a) after 5-month exposure, showing that the protective ability of the rust layer formed on weathering steel Q450NQR1 is superior to that on low-carbon steel Q235 in a shorter time.

3.2 Characteristics of the rust layer

3.2.1 Macro-morphologies of corrosion products

The variation in the appearance of the rust formed on carbon steel with exposure time is an intuitive concept. Figure 2 shows the evolution of the macro-morphologies of the corrosion products on Q235 and Q450NQR1 during rusting in the Spratly Islands atmospheric environment. It can be seen that the rust color on both steels became gradually darker with exposure time, from light yellow to orange, then to dull brown. Before 2-month exposure, the macro-morphologies of Q235 and Q450NQR1 were similar; there were a few uncorroded areas scattered on the sample surface after 15-d exposure, whereas 1 month later, a continuous rust layer completely covered the sample surface. The corrosion products began to accumulate locally on Q235 after 2-month exposure, whereas the corrosion products remained evenly distributed on Q450NQR1. As the exposure time continuously increased to 5 m and then 12 m, the color of the rust layer on Q235 became mixed with more yellow parts than that of Q450NQR1. Similarly, the rust color of Q450NQR1 was much darker, which may correspond to the formation of more Fe_3O_4 [23]. In addition, the corrosion product was more uniformly distributed. The difference may depend on the rust composition and the formation process of the corrosion products.

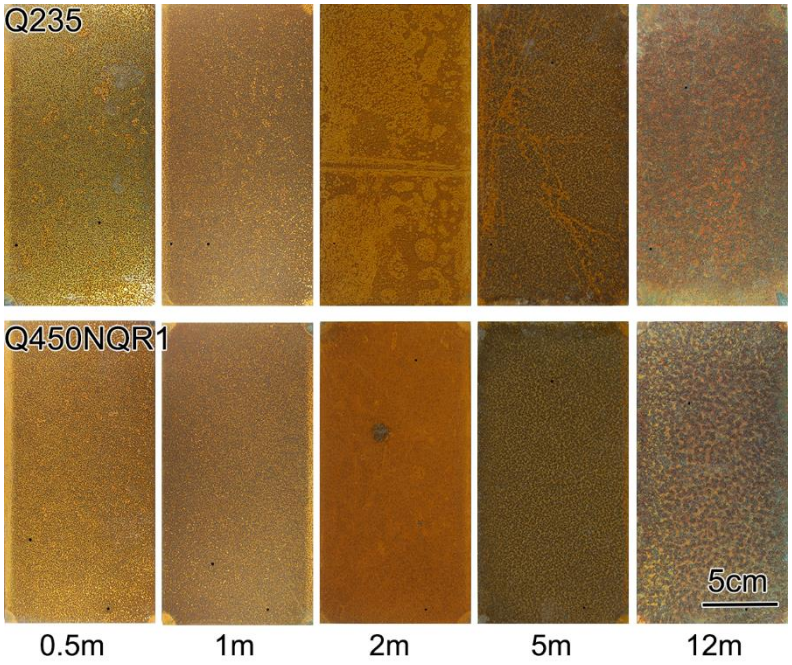

Figure 2. Evolution of the macro-morphologies of the corrosion products on Q235 and Q450NQR1 during its rust process

3.2.2 Micro-morphologies of corrosion products

The rust layers formed on steel exposed to the open-air environment were highly irregular, in general, with heavy cracking. In Figure 3, it is possible to see the variation in the structure of the rust

layer formed on both steels with exposure time. Figure 3(a), (c), and (e) show that the layer formed on Q235 was not uniform, being thicker in some local areas than in others, particularly at 5-month exposure. The thickness of the compact rust layer did not increase from 5 months to 12 months, which might be because of the exfoliation of the outer rust layer during the exposure process or poorly adhesive corrosion products during the transport process. This phenomenon might be caused by the changeable molar volume of the rust phase from the original iron or the initial corrosion products [17]. Thus, it cannot be seen clearly how much corrosion products have formed from the cross-section morphologies.

Figure 3(b), (d), (f) show the variation in the cross-section morphologies of the rust layer formed on Q450NQR1 during the 12-month exposure. Clearly, the structure and thickness of the rust layer after 2-month exposure were the same as that for Q235; however, after 5 m, the thickness of the rust layer was thinner, while as time advanced to 12 m, the rust layer became thicker and more compact compared to that of Q235. This did not indicate that the corrosion products formed on Q450NQR1 were less than those of Q235. Instead, it may be related to the peeling amount of the outer rust layer during exposure or the transport process, as shown in Figure 3(g) and Figure 3(h). Generally speaking, as a diffusion barrier, the rust layer could be assumed to hinder the infiltration of the corrosive medium; however, when the rust layer was wetted, the thick rust layer provided an area for the seawater to fill, slowing down water evaporation [24]. On the one hand, the porosity, spallation, fissure, and cracking distribution in the rust layer can be filled with water, in which the anodic dissolution of iron is balanced by the cathodic reduction of Fe^{3+} oxides in the rust layer; on the other hand, non-protective oxide layers can provide a channel for the penetration of aggressive agents, such as chloride ions and oxygen, to the metallic substrate, thereby increasing the corrosion rate.

Figure 4 shows the EDS spectra distribution in the rust layer. It can be seen that at the bottom of the rust layer, elemental Cl was detected on Q235, whereas a small amount of Cr was detected on Q450NQR1. As is well known, Cr is a powerful element to increase the corrosion resistance of weathering steel [22, 25]. Thus, the smaller corrosion rate of Q450NQR1 after 5-month exposure may be ascribed to the alloy element Cr, inhibiting Cl^- permeating to the substrate. In addition, the enrichment of Cr in the rust layer can promote compactness and lead to the thinning of corrosion product particles. Although Cu and Ni were not detected in this study, the influence of both alloy elements on improving the corrosion resistance cannot be ignored. Many studies have shown that Cr, Cu, Ni, and P can be enriched in the inner rust layer in different degrees, inhibiting oxygen diffusion to the steel surface and reducing rust conductivity. Thus, weathering steel with these alloyed elements exhibit high corrosion resistance in coastal atmospheres when a protective rust layer has formed after a long-term exposure [26-28].

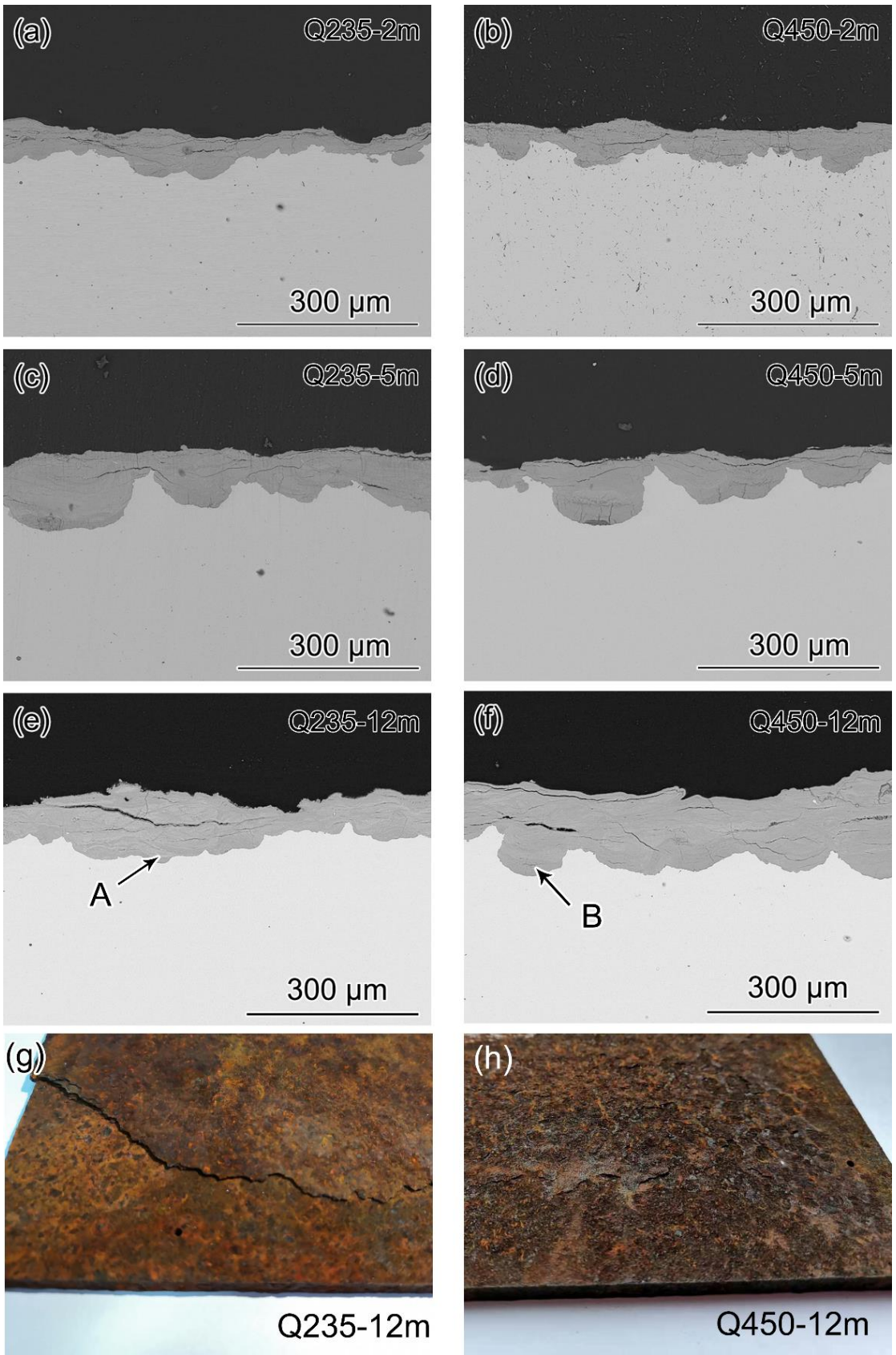

Figure 3. Characteristics of the rust layer structure formed on Q235 and Q450NQR1

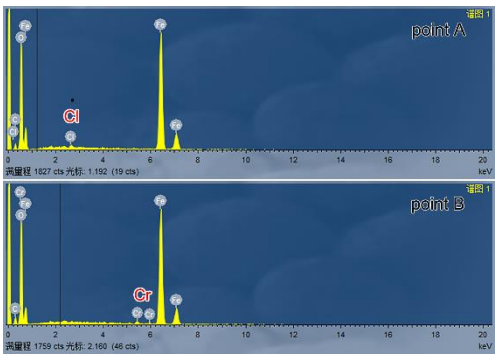

Figure 4. Element composition of points in **Figure 3**.

3.3 Composition of the rust layer

It is known that not only the structure of the rust layer but also the composition of corrosion product is closely related to the variation of the corrosion rate. Usually, atmospheric corrosion products of iron comprise various types of oxides, hydroxides, oxyhydroxides, and other complex forms. To explain the difference in corrosion rates between Q235 and Q450NQR1, and the variation of the corrosion rate with exposure time, the rust composition and relative content of each phase were analyzed by XRD and Maud refinement, shown in Figure 5.

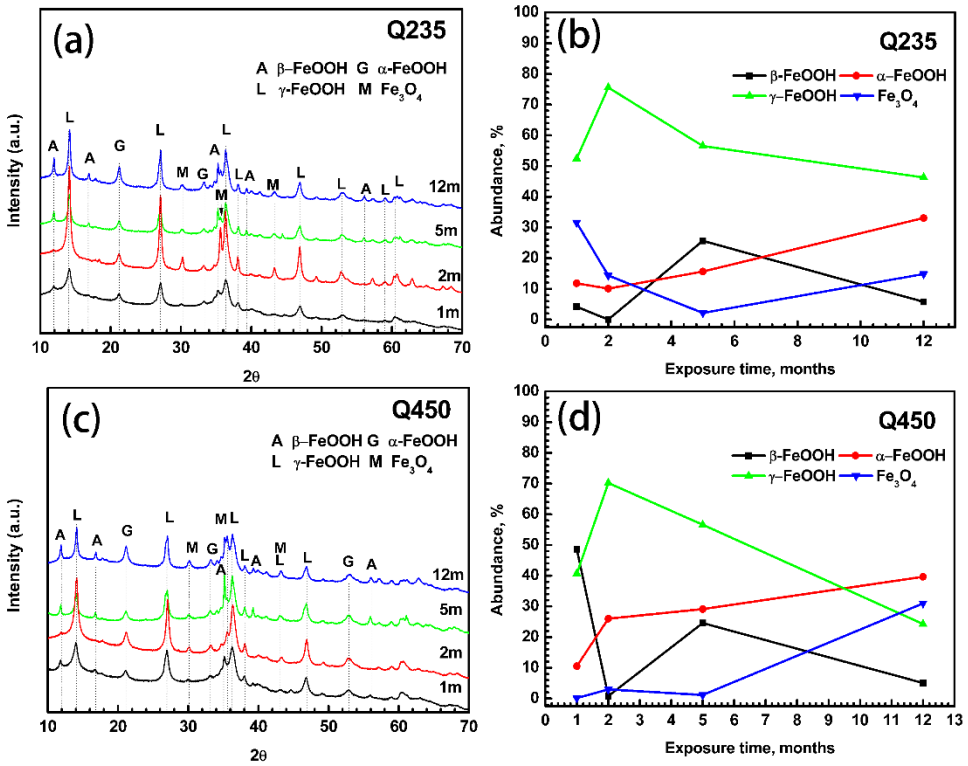

Figure 5. Variation in the composition of corrosion products and the relative amount of each phase as function of exposure time.

Figure 5(a) shows the rust layer composition formed on Q235 after 12-month exposure in the Spratly Islands. It can be seen that the corrosion products were mainly composed of β–FeOOH, α–FeOOH, γ–FeOOH, and Fe_3O_4 (or Fe_2O_3). Few changes were found in the product phase with time. Thus, the relative amounts of the four types of products during the different exposure periods were computed from Maud refinement. Figure 5(b) depicts the evolution of the relative amount of each phase during the 12-month exposure. It can be seen that the relative amount of γ–FeOOH is higher than 50% during the exposure periods, indicating that γ–FeOOH formed preferentially during the corrosion process. The relative amount of β–FeOOH was much higher after 5-month exposure, then decreased with the advancement of exposure time to 12 m. The variation in the relative amount of Fe_3O_4 was in contrast to that of β–FeOOH, whereas α–FeOOH as a stable phase [29] increased gradually. However, in this study, as the relative amount of α–FeOOH increased, the corrosion rate did not decrease.

As for Q450NQR1, the composition of the corrosion products was the same as that of Q235 (Figure 5(c)); the variation in the relative amount of each phase is shown in Figure 5(d). The relative amount of γ–FeOOH first increased to greater than 50% at 2 m and then decreased to less than 30% at 12 m. The relative amount of β–FeOOH fluctuated with exposure time, whereas the relative amounts of α–FeOOH and Fe_3O_4 increased gradually.

As indicated by the macro-morphology results, the corrosion products totally covered the sample after 1-month exposure, and the rust appearance varied with exposure time and steel type. As γ–FeOOH was the first phase formed on the steel, its relative amount increased as the rust layers became thicker. From 2-month exposure, the relative amount of γ–FeOOH decreased, to be partially transformed into goethite (α–FeOOH) [17]. With time, Fe_3O_4 can be formed by interaction of γ–FeOOH and β–FeOOH with iron; however, transformation from α–FeOOH is difficult [30]. These transformations between each phase promoted the corrosion process.

Compared between the composition of corrosion products formed on the surface of this two types of steel, after 5-month exposure, the sum amount of α–FeOOH and Fe_3O_4 formed on Q450NQR1 became larger than that of Q235. The new protective ratio α*/γ* proposed by Dillmann et al., should be greater than 2, for which the corrosion products can be protective [31].

$$\alpha^*/\gamma^* = (\alpha + Fe_3O_4))/(\gamma + \beta) \quad \text{(Eq.4)}$$

Table 3. Variation of the protective ability index ratios (α*/γ*)

Exposure time/months	1	2	5	12
Q235	0.767	0.323	0.217	0.921
Q450NQR1	0.120	0.408	0.435	2.41

The ratios for all corrosion products are provided in Table 3, which shows that the protective ability index ratio α*/γ* obtained was not greater than 2 for any period except for Q450NQR1 after 12-m exposure. Thus, the corrosion products in our study were not protective for any period except for Q450NQR1 after 12-month exposure. This is also the reason why the corrosion rate increased in all the periods for Q235, and the corrosion rate of Q450NQR1 increased before 5-m exposure, then decreased after 12-month exposure.

3.4 Electrochemical measurements

Atmospheric corrosion is essentially an electrochemical reaction between the metal and its surrounding environment, occurring on the substrate surface. Thus, electrochemical measurement is an efficient method to further understand the effect of the rust layer on the corrosion behavior of Q235 and Q450NQR1. In this study, a potentiodynamic polarization test on the rusted samples was conducted to understand the corrosion mechanism.

Figure 6 shows the potentiodynamic polarization curves of rusted Q235 and Q450NQR1 in 0.1 mol/L Na_2SO_4 solution. Comparing the rusted samples, we can clearly find that all polarization curves had similar shapes, implying similarities in the polarization behavior and corrosion mechanism. The cathodic process of both steels was controlled by charge transfer owing to the reduction of ferric rust [32, 33], and the anodic process was controlled by iron dissolution. Table 4 lists the values of the corrosion potential (E_{corr}) and corrosion current density (I_{corr}) obtained by the Tafel extrapolation from Figure 6. For low-carbon steel Q235, E_{corr} decreased from −537.63 mV to −589.93 mV, with the corresponding I_{corr} increasing from 80.08 μA·cm^{-2} to 354.0 μA·cm^{-2} with exposure time. The potentiodynamic polarization curve of Q235 shows that the corrosion potential shifted to the negative side gradually, and the anode current branch shifted to the right with exposure time. Combined with the corrosion kinetic result and the section morphologies of the rust, the dissolution of iron predominates the corrosion process, owing to the many cracks that existed in the rust layer, thereby promoting the corrosion medium permeating to the substrate of low-carbon steel Q235.

Meanwhile for Q450NQR1, E_{corr} increased from −594.64 mV to −428.22 mV, and the corresponding I_{corr} increased from 88.90 μA·cm^{-2} to 232.1μA·cm^{-2} then decreased to 205.4 μA·cm^{-2}.

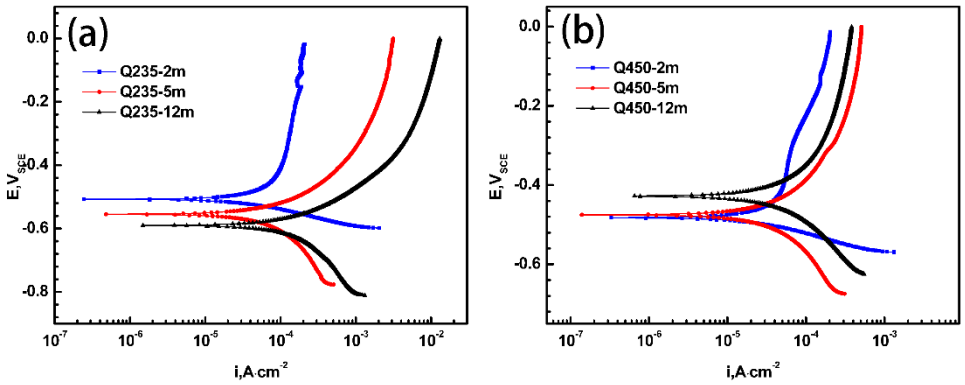

Figure 6. Potentiodynamic polarization curves of rusted Q235 and Q450NQR1

Table 4. Corrosion potential (E_{corr}) and corrosion current density (I_{corr}) obtained by Tafel extrapolation

Exposure time/m	Q235		Q450NQR1	
	E_{corr}/mV	I_{corr}/μA·cm^{-2}	E_{corr}/mV	I_{corr}/μA·cm^{-2}
2	−537.6	80.08	−594.6	88.90
5	−555.0	92.25	−475.4	232.1
12	−589.9	354.0	−428.2	205.4

After 5-month exposure, the corrosion potential E_{corr} of Q235 was more negative than that of Q450NQR1, and the corrosion current density I_{corr} was much larger after 12 months. As is well known, the corrosion current density I_{corr} is closely related to the corrosion rate. The variation of I_{corr} in this study was in good agreement with that calculated from the corrosion depth. All of the analysis results fully demonstrated the superiority of weathering steel used in this marine atmospheric environment after 12-month exposure.

3.5 Corrosion mechanism of low-carbon steel Q235 and weathering steel Q450NQR1

The corrosion reaction of metals is usually an electrochemical reaction under thin liquid film. When low-carbon steel Q235 was exposed to the Spratly Islands atmosphere with high humidity, many transformations may occur in the corrosion products layer due to the presence of different morphologies and type of corrosion products, as also contaminants. Fe was quickly oxidized to Fe^{2+}[17], transformed to $Fe(OH)_2$ or $FeOH^+$ by hydroxylation; then, it reacted to form γ-FeOOH by preferential oxidation of $FeOH^+$ with oxygen dissolved in the thin liquid [25]. When Cl^- was abundant, $FeCl^+$ was generated, then transformed to β-FeOOH. As time advanced, γ-FeOOH, as a strong reducibility intermediate, can be transformed to α–FeOOH, whereas reduction back to Fe_3O_4 is also a possibility [34]. A pathway to β-FeOOH through re-crystallization is also available [35]. Fe_3O_4 can be formed by the interaction of β-FeOOH with iron. In the Spratly Islands tropical marine atmosphere, the corrosion evolution of low-carbon steel Q235 in 1-y exposure is a continuously accelerated process. This is mainly because the electrochemical reaction processes can be greatly promoted by a continuously high temperature (average temperature 28.1 °C); meanwhile, the transformation between different corrosion products can also be promoted. In the composition of corrosion products, the density of Fe_3O_4 is higher than that of FeOOH, which induced the exfoliation of the local rust layer, reported in Section 3.2.2. The porous rust layers can lock the water, enhancing the transport of oxygen to the metal surface and promoting the adsorption and dissolution of the chloride ion. The relative humidity at this atmosphere is relatively high (average 81.6%), which further intensifies the adsorption of water and chloride ion, accelerating the corrosion process. Due to the characteristics of the atmospheric environment in Spratly Islands, all the chemical and electrochemical reactions which involved in the corrosion products layer can be promoted.

For weathering steel Q450NQR1, the initial corrosion reaction process before 2-month exposure was similar to that of Q235. With exposure time, the alloy elements Cr, Ni, and Cu increased the corrosion resistance of weathering steel to some extent by improving the density of the rust layer and inhibiting Cl^- permeating to the substrate, which lowered the formation rate of β-FeOOH. Thus, the relative composition of each product was different from that of Q235. The effect of alloying elements was more obvious after 12 months, with Cr accumulated in the inner layer (see **Figure** 3(f) and **Figure** 4), further enhancing the corrosion resistance. Although Cu was not detected, Cu^+ was found to be involved in the formation of inverse spinel oxide Fe_3O_4 [36, 37]. The relative composition of Fe_3O_4 increased gradually, and the protective ability index ratio α*/γ* increased to greater than 2, which reduced the corrosion rate after 12 months.

4. CONCLUSION

The followings are the main conclusion of this research:

1. For initial corrosion stages of both steels, the kinetics of corrosion process follow exponential function $D=At^n$, both corrosion processes were accelerated trends. But the corrosion rate of Q235 increased continuously during 12 months exposure, and the corrosion rate of Q450NQR1 first increased and then decreased slightly. According to corrosion rate, r_{corr} for the first year of exposure for different corrosivity categories defined in ISO 9223, r_{corr} of low carbon steel Q235 exposed to Spratly Islands was 237.5μm/a, therefore the corrosivity category of this marine atmosphere CX.
2. The rust color of both steels became darker as exposure time prolonged, from light yellow to orange, then to dull brown. After 5 months exposure, the rust layer of Q450NQR1 was more uniform.
3. The porosity, spallation, fissure and cracking distributing in the rust layer allow aggressive agents, such as chloride ions and oxygen, easy access to the metallic substrate, thereby increasing corrosion rate.
4. The rust phases formed on both steels were basically same, respectively β–FeOOH, α–FeOOH, γ–FeOOH and Fe_3O_4, the relative amount of each phase formed on both steels changed as time processes. The protective ability index ratio α*/γ* obtained was not over 2 for all periods except that of Q450NQR1 after 12 m exposure.
5. As exposure time progresses, the corrosion current density I_{corr} of Q235 was gradually incrased, while I_{corr} of Q450NQR1 was first increased then decreased slightly.
6. In this tropical marine atmosphere, weathering steel Q450NQR1 performed better corrosion resistance than low carbon steel Q235 after 5 months.

ACKNOWLEDGEMENTS
The investigation was supported by Strategic Priority Research Program of the Chinese Academy of Sciences (No. XDA13040502) and National Natural Science Foundation of China (No. 51671197) and (51601199).

References

1. W. Hou, C. Liang, *Corrosion*, 55 (1999) 65.
2. S.J. Oh, D.C. Cook, H.E. Townsend, *Corros. Sci.*, 41 (1999) 1687.
3. H.E. Townsend, *Corros.*, 57 (2001) 497.
4. Q.C. Zhang. J. S. Wu, J. J. Wang, W. L. Zheng, J.G. Chen, A.B. Li, *Mater. Chem. Phys.*, 77 (2002) 603.
5. B.Y.R. Surnam, C.V. Oleti, *Corros. Eng., Sci. Technol*, 47 (2013) 446.
6. M. Morcillo, B. Chico, L. Mariaca, E. Otero, *Corros. Sci.*, 42 (2000) 91.
7. D. de la Fuente, I. Díaz, J. Simancas, B. Chico, M. Morcillo, *Corros. Sci.*, 53 (2011) 604.
8. B.R. Demeybaum, E.S. Ayllon, *Corrosion*, 36 (1980) 345.
9. M. Morcillo, B. Chico, J. Alcántara, I. Díaz, J. Simancas, D. de la Fuente, *Mater. Corros.*, 66 (2015) 882.
10. E. Almeida, M. Morcillo, B. Rosales, *Br. Corros. J.*, 35 (2000) 284.
11. W. Han, C. Pan, Z. Y. Wang, G. C. Yu, *J. Mater. Eng. Perform.*, 24 (2014) 864.
12. M. Morcillo, B. Chico, D. de la Fuente, J. Simancas, *Int. J. Corros.*, 2012 (2012) 1.

13. R. Ericsson, *Werkst. Korros.-Mater. Corros.*, 29 (1978) 400.
14. F.C. Perez, *Corrosion*, 40 (1984) 170.
15. M. Morcillo, J. Alcántara, I. Díaz, B. Chico, J. Simancas, D. De la Fuente, *Rev. Metal.*, 51 (2015) e045.
16. S. Feliu, M. Morcillo, B. Chico, *Corrosion*, 55 (1999) 883.
17. J.C. Guerra, A. Castañeda, F. Corvo, J.J. Howland, J. Rodríguez, *Mater. Corros.*, 70 (2019) 444.
18. J. Alcántara, B. Chico, I. Díaz, D. de la Fuente, M. Morcillo, *Corros. Sci.*, 97 (2015) 74.
19. X.G. Li, Dong, C. F., Xiao, K., Gao, J., Typical materials corrosion /aging behavior and mechanism at Xisha marine atmospheric environment, science press, Beijing, 2014.
20. V. Kucera, D. Knotkova, J. Gullman, P. Holler, *Key Eng. Mater.*, 20-28 (1991) 167.
21. Q. H. Tang, J. N. Li, H. Dai, *Equip. Environ. Eng.*, 7 (2010) 1.
22. M. Yamashita, H. Miyuki, Y. Matsuda, H. Nagano, T. Misawa, *Corros. Sci.*, 36 (1994) 283.
23. J. Alcantara, D. Fuente, B. Chico, J. Simancas, I. Diaz, M. Morcillo, *Materials*, 10 (2017)1.
24. X. Zhang, S. W. Yang, W. H. Zhang, H. Guo, X. L. He, *Corros. Sci.*, 82 (2014) 165.
25. T. Misawa, K. Asami, K. Hashimoto, S. Shimodaira, *Corros. Sci.*, 14 (1974) 279.
26. K. Asami, M. Kikuchi, *Corros. Sci.*, 45 (2003) 2671.
27. F. Iwei, *Br. Corros. J.*, 26 (2013) 209.
28. M. Stratmann, K. Bohnenkamp, T. Ramchandran, *Corros. Sci.*, 27 (1987) 905.
29. Z. Wang, J. Liu, L. Wu, R. Han, Y. Sun, *Corros. Sci.*, 67 (2013) 1.
30. M. Morcillo, J.M. González-Calbet, J.A. Jiménez, I. Díaz, J. Alcántara, B. Chico, A. Mazarío-Fernández, A. Gómez-Herrero, I. Llorente, D. de la Fuente, *Corrosion*, 71 (2015) 872.
31. P. Dillmann, F. Mazaudier, S. Hœrlé, *Corros. Sci.*, 46 (2004) 1401.
32. T. Nishimura, H. Katayama, K. Noda, T. Kodama, *Corrosion*, 56 (2000) 935.
33. I. Matsushima, T. Ueno, *Corros. Sci.*, 11 (1971) 129.
34. Y.Y. Chen, H.J. Tzeng, L.I. Wei, L.H. Wang, J.C. Oung, H.C. Shih, *Corros. Sci.*, 47 (2005) 1001.
35. T. Misawa, K. Hashimoto, S. Shimodaira, *Corros. Sci.*, 14 (1974) 131.
36. L. Hao, S. X. Zhang, J. H. Dong, W. Ke, *Corros. Sci*., 53 (2011) 4187.
37. W. Ke, J. H. Dong, *Acta Metall. Sin.(Engl. Lett.)*, 46 (2010) 1365.